

Full length article

Design method of axial compression stability for cross-section corrugated plate steel special-shaped column

Zi-qin Jiang ^{a,b,*}, Zi-yao Niu ^a, Ai-Lin Zhang ^{a,b,c}, Xue-chun Liu ^{a,b}^a College of Architecture and Civil Engineering, Beijing University of Technology, Beijing, 100124, China^b Beijing Engineering Research Center of High-Rise and Large-Span Prestressed Steel Structure, Beijing, 100124, China^c Beijing Advanced Innovation Center for Future City Design, Beijing, 100044, China

ARTICLE INFO

ABSTRACT

Keywords:

Cross-section special-shaped column
Corrugated plate steel structure
Axial compression stability
Flexural buckling
Torsional buckling
Design method

Obtaining a larger moment of inertia and overall stability with smaller material input, which is an effective way to improve the bearing capacity and reduce the self-weight of structural columns. This paper proposes a cross-section corrugated plate steel special-shaped column (CCSC), which is based on the optimization design idea of steel profiled-shaped column section, combined with the comprehensive consideration of the overall stability of steel structure column members, material use efficiency and building interior space utilization rate. The new CCSC is composed of three parts: core square steel pipe, corrugated plate, and flange plate. The high-out-of-plane stiffness characteristic of corrugated plate is utilized to improve the section rotation radius. The three parts above are coordinated to resist lateral load. The square steel pipe and flange plate are the main vertical bearing plates. The new special-shaped column can obtain a larger moment of inertia and overall stability with a smaller material input, thus improving the bearing capacity. Through the combination of theoretical analysis and numerical simulation, the overall stability of the axial compression of CCSC are analyzed, and the instability modes and failure modes of CCSC are revealed. The design method and suggestions for the stability of CCSC under axial compression are put forward. Then, the overall stability design and application suggestion based on conventional square steel tube is given. The results show that the stability design method of CCSC under axial compression can effectively judge the instability mode of CCSC and obtain the ultimate bearing capacity of the whole member. Compared with square steel tube columns with regularized slenderness ratio greater than 0.8 in structural design, the CCSC has obvious advantages in overall stability and steel consumption.

1. Introduction

The traditional construction mode, which is characterized by high energy consumption and pollution, is fully incompatible with the modern values of the current era, which emphasizes applicability, efficiency, sustainability, and development. The standardized design, factory production, short construction periods, and lightweight materials of steel structures have become the new direction and trend in construction development, with the potential to improve efficiency and reduce environmental impact [1–3]. As the proportion of high-rise buildings in urban areas continues to rise, there is an imminent need for research aimed at improving the performance and self-weight optimization of steel structural members.

The current trend of utilizing special shaped columns presents an optimal solution for improving the comprehensive performance and

upgrading of structural columns, showcasing their immense potential for application. With an innovative column section design, it seamlessly integrates into the wall section, avoiding column protrusion and significantly enhancing the efficiency of indoor space utilization. The targeted strengthening or economic design of the special shaped column section can be executed based on the structural stress characteristics, to ensure safety while improving the efficiency of building material usage and product economy [4–6]. The research and application achievements have matured in the field of reinforced concrete special-shaped columns and concrete-filled steel tube special-shaped columns in high-rise buildings. Due to the good plasticity of steel and concrete, there is a continuous output of innovative research results in this topic [7–9]. As for pure steel structures, steel special-shaped columns have been extensively used in multi-story residential buildings, with mature design concepts of beam-column connection joints and supporting steel frames.

* Corresponding author.

E-mail address: jzqbj2010@163.com (Z.-q. Jiang).

When compared to traditional square and round steel columns, special shaped columns exhibit notable advantages in strength and stiffness, and can have more steel arranged on the outer edge of the cross-section, providing exceptional and reliable ductility and hysteresis performance during earthquakes [10–14]. With the increasing load design values in the current development of high-rise buildings, it is necessary to develop special shaped steel columns with higher overall stability. The special-shaped column can realize the optimization of structure self-weight with the combination of material-saving connector and bearing plate [15]. However, the current special shaped steel columns have a singular cross-sectional form, and larger cross-sectional heights necessitate a larger web thickness [16], diminishing the steel utilization efficiency to some extent.

Corrugated plates, as a typical form of material-saving plates, have many targeted application characteristics in the construction industry. On the one hand, the corrugated plate is difficult to transfer the stress in the direction of the waveform, but has good deformation ability and ductility. On the other hand, corrugated plates have a large out-of-plane stiffness, and their height-to-thickness ratio can reach $600\sqrt{235/f_y}$, far exceeding that of conventional flat steel plates [17]. Thus, when corrugated plates are used as web plates in beam and column members, the section height of the members can be effectively increased with a small rise in material cost, improving the shear bearing capacity and overall stability of the members [18]. Based on these advantages, using corrugated plates instead of flat plates as the traditional welded I-section web plates can reduce the amount of steel used. Scholars at home and abroad have conducted a lot of theoretical and experimental research on this type of corrugated web plate I-section member, proving its good performance in flexural, shear, compression and torsion [19–21]. Numerous tests or simulation studies have shown that this type of structural member can meet the relevant functional requirements such as structural columns, beams and connecting beams, and has significant performance or cost advantages over conventional I-shaped section members [22–26]. The related design and calculation methods are constantly being improved, with theoretical calculation results becoming more consistent with actual situations [27]. Based on the research on corrugated web plate I-section members, Jiang et al. [28–30] applied them to steel structure beam-column joints and frames, and conducted a comprehensive analysis on the application of corrugated web plate I-section members through experiments and simulations. Their research results proved that this type of member can match well with connecting members, providing a reliable theoretical basis for promotion in the engineering industry. Similar to the design idea of corrugated web plate I-section members, corrugated web plate box-section members form a corrugated plate application scheme based on conventional box sections, which also exhibit the characteristics of large section height and steel saving [31]. In addition, some scholars have used the large out-of-plane stiffness of corrugated plates to increase the lateral stiffness of column members by using them as column wall plates [32–34], or to enhance the energy dissipation capacity of shear wall members by taking advantage of their strong deformation ability and resistance to buckling [35–39]. Although some innovative structures have been developed, their popularity has been poor, and the application forms of corrugated plates in the construction field are still relatively simple. Currently, most of the related members with corrugated plates have irregular surfaces, making it difficult to connect with other members, which further hinders the popularization of this type of material-saving plate.

To provide a solution to the above issues, we propose a cross-section corrugated plate steel special-shaped column (CCSC), which is based on the optimization design idea of steel profile-shaped column section, combined with the comprehensive consideration of the overall stability of steel structure column members, material use efficiency, and building interior space utilization rate. This new special-shaped column is composed of three parts: core square steel pipe, corrugated plate and

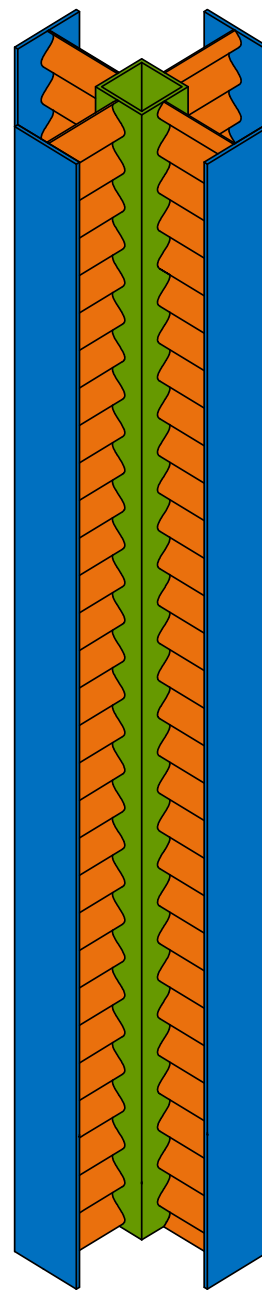


Fig. 1. Construction of CCSC.

flange plate, as shown in Fig. 1. The column features a corrugated plate as the web and a core square steel pipe to complete orthogonal connections between the corrugated plate sections. The corrugated plate is incorporated to improve the section rotation radius. The square steel pipe and flange plate are the main vertical bearing plates. All of the above three parts are coordinated to resist lateral load. The column design fully utilizes the high-out-of-plane stiffness characteristic of the corrugated plate, increases the width-thickness ratio of the corrugated plate section, significantly enhances the section height with less steel used in the corrugated plate, and ultimately achieves the improvement of overall stability and self-weight optimization of the column member. The CCSC can be embedded inside the wall, with its central cavity and peripheral open cross-section meeting the space requirements of pipeline arrangement and ensuring that the interior space and aesthetics are not compromised. This paper combines theoretical analysis and numerical simulation to evaluate the overall axial stability and strength of the cross-section corrugated plate steel special-shaped column, thus

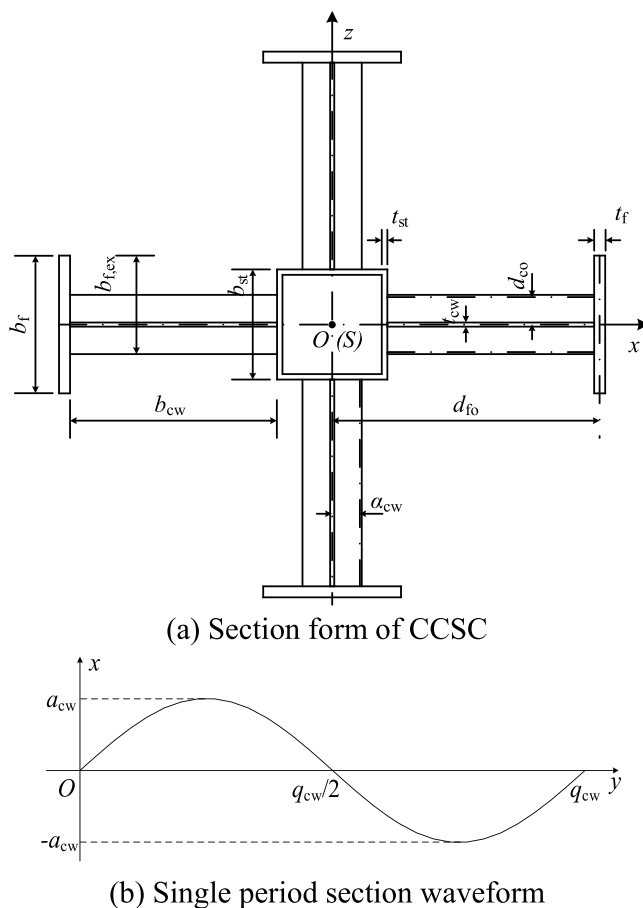


Fig. 2. Section composition of CCSC.

providing design methods and suggestions for axial stability.

2. Composition and parameters of CCSC

The CCSC is mainly composed of three parts: core square steel pipe, corrugated plate and flange plate. The square steel pipe is welded with four corrugated plates, and the flange plates are welded with corrugated plates. The section form of CCSC is shown in Fig. 2a. The parameters b_{st} and t_{st} respectively represent the section outer side length and wall thickness of the square steel pipe; b_f and t_f respectively represent the section width and thickness of flange plate; $b_{f,ex}$ represents the maximum extension width of flange plate section, which can be obtained by Eq. (1); b_{cw} and t_{cw} respectively represent the section width and thickness of corrugated plate; the point $O(S)$ is the centroid (shear center) without the consideration of corrugated plates; d_{fo} represents the distance between the central axis of flange plate section and the central axis of the overall section; d_{co} represents the deviation distance between the central axis of the corrugated plate section at any height the column and the central axis of the overall section.

The corrugated plate adopts sinusoidal waveform section, as shown in Fig. 2b. The parameters a_{cw} and q_{cw} respectively represent the amplitude and wavelength of the waveform. The approximate value of the expansion length of the single period h_{cw} can be calculated by Eq.

(2). The equivalent full-section area of the CCSC A_{equ} can be obtained by Eq. (3), where A_{st} and A_f respectively represent the section area of the square steel pipe and a single flange plate. The width and thickness ratio of square steel pipe and flange plate are expressed by α_{st} and α_f respectively. The calculation method is shown in Eq. (4) and Eq. (5).

$$b_{f,ex} = (b_f - t_{cw})/2 + a_{cw} \quad (1)$$

$$h_{cw} = q_{cw} \left(3.88 \frac{a_{cw}^2}{q_{cw}^2} + 1.07 \frac{a_{cw}}{q_{cw}} + 0.95 \right) \quad (2)$$

$$A_{equ} = A_{st} + 4A_f + 4 \frac{h_{cw}b_{cw}t_{cw}}{q_{cw}} \quad (3)$$

$$\alpha_{st} = (b_{st} - 2t_{st})/t_{st} \quad (4)$$

$$\alpha_f = b_{f,ex}/t_f \quad (5)$$

3. Failure mode analysis of axial compression

3.1. Finite element model design

The finite element analysis software ABAQUS[40] is used to establish the numerical model of CCSC, with the mesh of S4R shell element and tie interaction among the plates. The hinged displacement boundary conditions are set at both ends of the column. Specifically, the boundary conditions are as follows: the displacement of the column end in all directions is limited except the direction of the loading direction on the column top, and the rotation of the column end is free expect the rotation around the longitudinal axis. The loading point of the model is located at the center of the top of the column, and the loading direction is negative of the Y-axis. The trial example model Column-1 and Column-2 are designed according to Table 1 to study the failure mode of CCSC, where H_c represents the height of the special-shaped column model, and f_y represents the yield strength of the model material. The material constitutive model is an ideal elastic model, with the elastic modulus at 206 GPa and Poisson's ratio at 0.3. According to T/CECS 290–2022 “Technical specification for steel corrugated-plates structures” [17], $a_{cw} = 20\text{mm}$ and $q_{cw} = 150\text{mm}$.

3.2. Failure mode analysis

In this paper, the possible global instability mode of CCSC under axial compression is studied through elastic buckling analysis. The first buckling mode obtained from the elastic buckling analysis of each model is applied as the initial defect[41], so as to study the failure mode of CCSC under the elastoplastic condition. The initial geometric imperfection value applied to the model is $H_c/500$ [42]. The axial load is applied to the model in the way of displacement loading. The loading vertical displacement is 1% of the column height, that is, the axial compressive strain of the model is 1%.

The axial compression failure modes of Column-1 and Column-2 are shown in Fig. 3. It can be seen from the results of elastic buckling analysis that there are two axial buckling modes: flexural buckling and torsional buckling. It can be seen from the results of elastoplastic static analysis that flexural instability occurs on the model Column-1 with an obvious flexural phenomenon and serious stress concentration, and the material near the column end is in elastic state. Torsional instability

Table 1
Parameters of the pilot model.

Model	H_c (mm)	b_{st} (mm)	t_{st} (mm)	b_f (mm)	t_f (mm)	b_{cw} (mm)	t_{cw} (mm)	f_y (MPa)
Column-1	6000	100	5	150	12	150	3.0	345
Column-2	6000	100	5	150	12	200	3.0	345

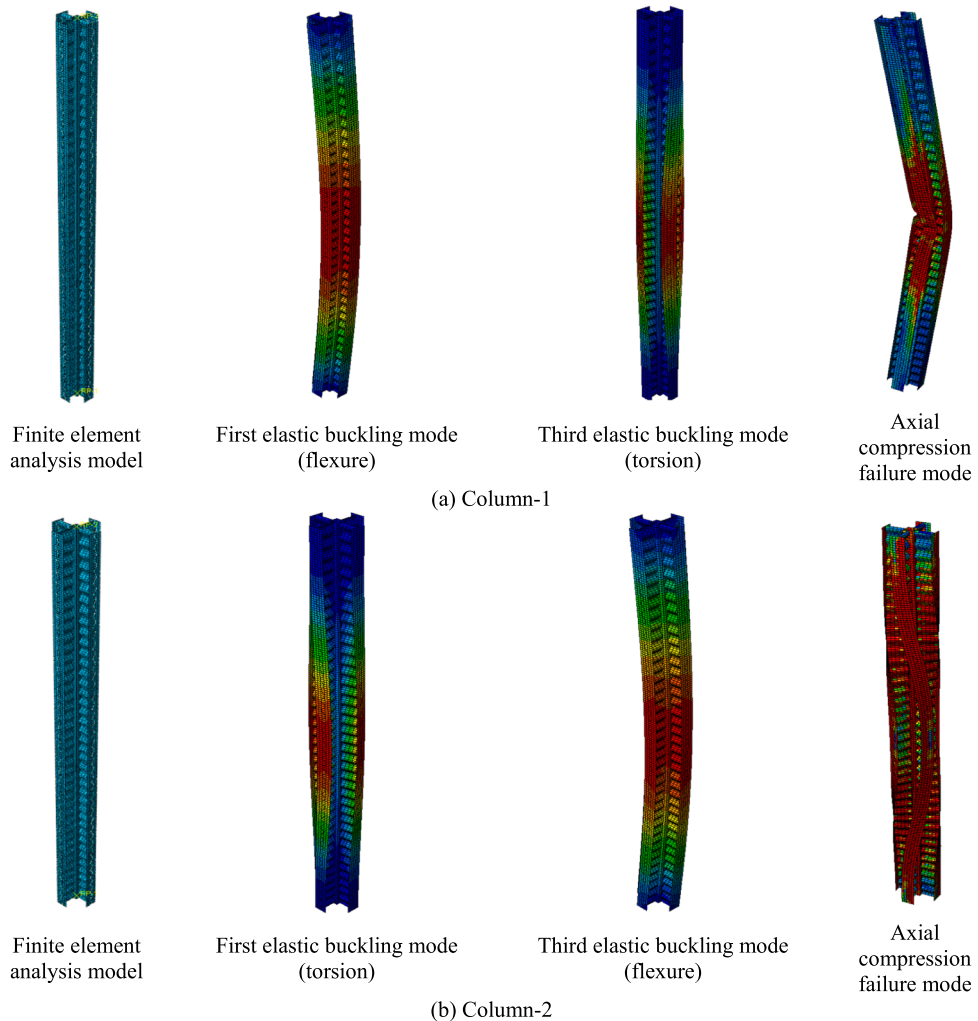


Fig. 3. Axial compression failure mode of CCSC.

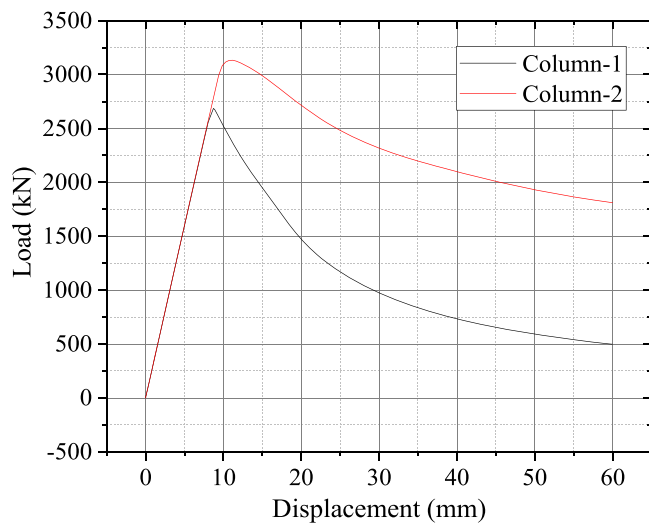


Fig. 4. Axial compression load-displacement curve.

occurs on the model Column-2 with a relatively uniform overall deformation, and the whole square steel pipe and flange plate almost enter the plastic stage. The correlation curve between the displacement of loading point and bearing capacity in the loading process is shown in

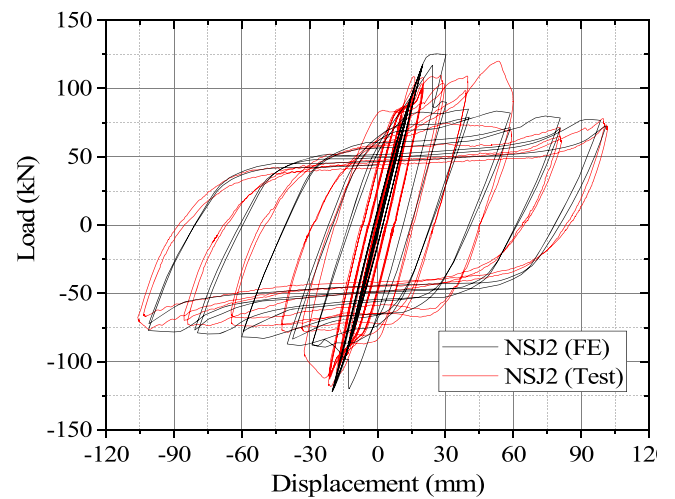


Fig. 5. Curve comparison between test and simulation.

Fig. 4. It can be seen that the peak value of Column-1 curve presents a sharp shape, while the peak value of Column-2 curve shows a smooth shape. This indicates that the bearing capacity of the column with flexural failure is reduced at a higher rate than that of the column with torsional failure, and has poorer ductility.

Table 2Parameters of auxiliary models for $k_{\text{cr,nb}}$.

Model	H_c (mm)	b_{st} (mm)	t_{st} (mm)	b_f (mm)	t_f (mm)	b_{cw} (mm)	t_{cw} (mm)	f_y (MPa)	α_{st}	α_f	$\lambda_{\text{b,n}}$
BB1_1~6	3000~6000	100	5	200	16	100	2.0	345	18	7.4	26~54
BB2_1~6	3000~6000	100	5	200	16	150	2.5	345	18	7.4	20~42
BB3_1~6	3000~6000	100	5	150	12	100	2.0	345	18	7.8	29~59
BB4_1~6	3000~6000	150	8	200	16	100	2.0	345	16.75	7.4	24~50
BB5_1~6	3000~6000	150	8	200	16	150	2.5	345	16.75	7.4	20~41
BB6_1~6	3000~6000	150	8	200	16	100	2.0	345	16.75	7.4	16~34
BB7_1~6	3000~6000	80	4	100	8	100	2.0	345	18	8.6	33~67
BB8_1~6	3000~6000	80	4	110	8	100	2.0	345	18	9.2	32~66
BB9_1~6	3000~6000	80	4	120	8	100	2.0	345	18	9.8	32~65
BB10_1~6	6000~9000	100	5	200	16	100	2.0	345	18	7.4	53~80
BB11_1~6	6000~9000	100	5	200	16	150	2.5	345	18	7.4	41~63
BB12_1~6	6000~9000	80	4	100	8	100	2.0	345	18	8.6	66~101
BB13_1~6	6000~9000	80	4	100	8	75	1.5	345	18	8.6	79~120
BB14_1~6	6000~9000	80	4	100	8	50	1.5	345	18	8.6	97~147
BB15_1~6	6000~9000	80	4	100	8	160	2.5	345	18	8.6	47~72
BB16_1~6	6000~9000	150	8	100	8	240	3.0	345	16.75	8.6	39~60
BB17_1~6	3000~6000	100	5	200	16	100	2.0	235	18	7.4	26~54
BB18_1~6	3000~6000	80	4	120	8	100	2.0	235	18	9.8	32~65
BB19_1~6	3000~6000	150	8	200	16	150	2.5	390	16.75	7.4	20~41
BB20_1~6	6000~9000	80	4	100	8	75	1.5	390	18	8.6	79~120
BB21_1~6	3000~6000	100	4	150	10	100	2.0	345	23	8.6	29~59
BB22_1~6	6000~9000	150	5	120	8	240	2.0	345	28	9.8	34~52

3.3. Finite element model verification

In order to verify the reliability of the finite element model, numerical model of prefabricated sinusoidal corrugated web beam-column joint specimen NSJ2 of Jiang et al. [29] was established using the same modeling method as in this paper. The comparison results of the hysteresis curve of NSJ2 between the numerical simulation and test result are shown in Fig. 5, where "FE" represents the finite element model and "Test" represents the test specimen. It can be seen from the figure that the finite element simulation results are in good agreement with the test results, indicating that the finite element model adopted in this paper has good accuracy and reliability.

4. Critical loads of elastic buckling

4.1. Basic assumption

The compressive and tensile strengths of corrugated plates are low, and corrugated plates will cause the section of columns to constantly change along the height. The theoretical equations in this paper are deduced based on the following assumptions:

- (1) The corrugated plate does not participate in the behavior of overall tensile and compressive strengths of the CCSC;
- (2) The section thickness of the corrugated plate part is always the same as the actual thickness of the corrugated plate;
- (3) The position change of the corrugated plate section along the column is ignored. The section of CCSC is a biaxial symmetric section, and the centroid and shear center of the section coincide with that of the square steel pipe;
- (4) The section of CCSC does not distort in the process of torsion.

4.2. Critical load of flexural buckling

4.2.1. Theoretical calculation equation of flexural buckling critical load

The Euler formula is mainly applicable to the calculation of the flexural buckling critical load of slender rod. To facilitate the design and calculation, the uniform calculation equation of the flexural buckling critical load $N_{\text{cr,nb}}$ of CCSC is proposed for both the slender rod and the non-slender rod, as shown in Eq. (6). $N_{\text{cr0,nb}}$ denotes the Euler critical load of flexural buckling of the axial compression column, and $k_{\text{cr,nb}}$ is

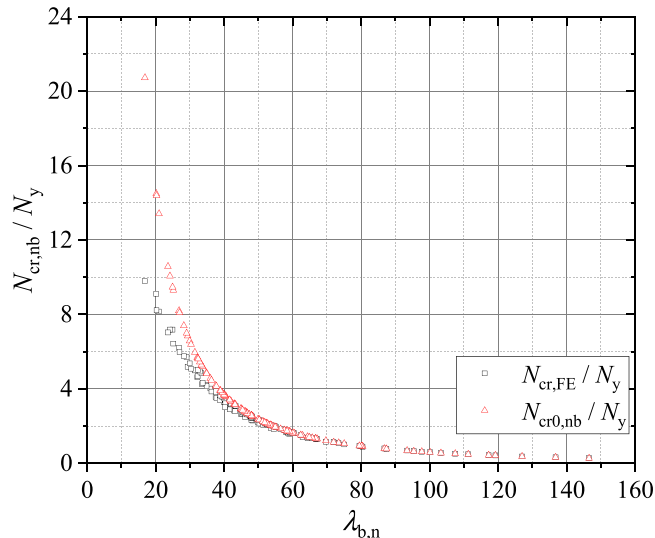


Fig. 6. Ideal elastic stability factor.

the adjustment factor of buckling critical load. The flexural slenderness ratio of CCSC $\lambda_{\text{b,n}}$ is calculated by Eq. (7), where l_{ob} is the effective length of the column while considering the boundary conditions of flexural deformation. The calculation of the section radius of rotation i_x can be performed by Eq. (8), where the section moment of inertia I_x and the net section area under compression A_{net} should ignore the corrugated plate.

$$N_{\text{cr,nb}} = k_{\text{cr,nb}} \cdot N_{\text{cr0,nb}} = k_{\text{cr,nb}} \cdot \frac{\pi^2 E A_{\text{net}}}{\lambda_{\text{b,n}}^2} \quad (6)$$

$$\lambda_{\text{b,n}} = l_{\text{ob}} / i_x \quad (7)$$

$$i_x = \sqrt{I_x / A_{\text{net}}} \quad (8)$$

4.2.2. Adjustment factor of flexural buckling critical load

The results of numerical simulation and theoretical calculation are compared and analyzed. The models designed according to Table 2 are used for data fitting of the adjustment factor of flexural buckling critical load $k_{\text{cr,nb}}$. Each group contains six models, and the design variables of

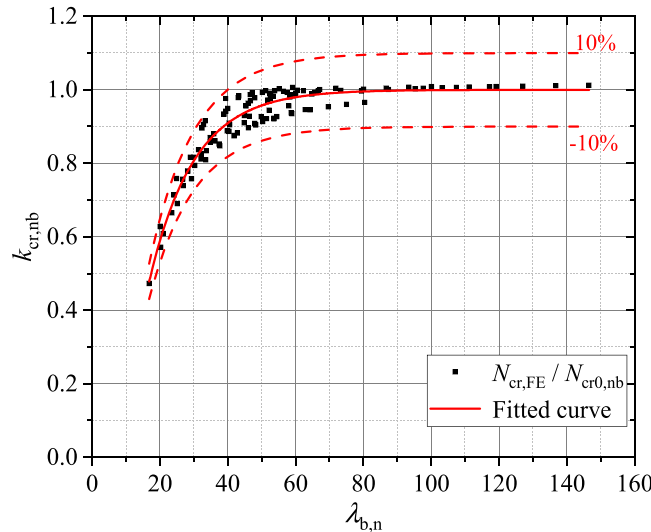


Fig. 7. Fitting process of $k_{cr,nb}$.

each group mainly considers the flexural slenderness ratio $\lambda_{b,n}$ of the column. The specific variable parameters are b_{st} , t_{st} , b_f , t_f , b_{cw} , t_{cw} and f_y .

The comparison between the results of Euler formula and finite element simulation of flexural buckling critical load of CCSC is shown in Fig. 6, where $N_{cr,FE}$ represents the numerical simulation results of critical elastic buckling load corresponding to each model, N_y represents the yield load of the full section of the axial compression member, and the calculation method is shown in Eq. (9). It can be seen that the Euler formula achieves good calculation accuracy when the slenderness ratio $\lambda_{b,n}$ is large, while it yields poor calculation accuracy when the slenderness ratio $\lambda_{b,n}$ is small.

The ratio of numerical simulation results $N_{cr,FE}$ to the Euler formula results $N_{cr0,nb}$ is the value of factor $k_{cr,nb}$. Taking the flexural slenderness ratio $\lambda_{b,n}$ as the main variable, the calculation equation of factor $k_{cr,nb}$ was obtained through data fitting, and the calculation error was reasonably kept within 10%, as shown in Fig. 7 and Eq. (10). With the increase in slenderness ratio $\lambda_{b,n}$, the value of factor $k_{cr,nb}$ gradually stabilizes to 1.0, which conforms to the variation rule of Euler formula calculation accuracy.

$$N_y = f_y \cdot A_{net} \quad (9)$$

$$k_{cr,nb} = 1.0 - 1.86 \times 0.927^{\lambda_{b,n}} \quad (10)$$

4.3. Critical load of torsional buckling

4.3.1. Free torsion constant and sectorial moment of inertia

For the open thin-walled member consisting of narrow and long rectangular sections, the free torsion constant $I_{t,rec}$ can be approximated by Eq. (11), where b_i denotes the width and t_i denotes the thickness of the rectangular section. The general equation for calculating the sectorial moment of inertia I_ω is shown in Eq. (12), where ω_n represents the main sectorial coordinate of the thin-walled section and can be calculated by Eq. (13), s represents the line integral length, t represents the thickness, and A represents the area. For a biaxial symmetric section, $\omega_n = \omega_s$, then ω_s , then ω_s itself is the main sectorial coordinate ω_n . Let the main sectorial coordinates at both ends of the rectangular section ($b_i \times t_i$) be ω_{ni} and ω_{ni+1} respectively, then the sectorial moment of inertia I_ω

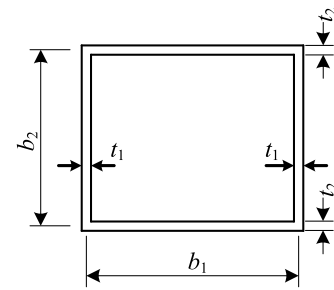


Fig. 8. General box section.

of the whole section can be expressed by Eq. (14).

$$I_{t,rec} = \frac{1}{3} \sum_{i=1}^n b_i t_i^3 \quad (11)$$

$$I_{\omega,rec} = \int_0^s \omega_n^2 t ds = \int_A \omega_n^2 dA \quad (12)$$

$$\omega_n = \omega_s - \frac{\int_A \omega_s dA}{A} \quad (13)$$

$$I_{\omega,rec} = \int_0^s \omega_n^2 t ds = \int_0^{l_i} \left(\omega_{ni} + \frac{\omega_{ni+1} - \omega_{ni}}{l_i} s \right)^2 b_i ds \\ = \frac{1}{3} \sum (\omega_{ni}^2 + \omega_{ni}\omega_{ni+1} + \omega_{ni+1}^2) t_i b_i \quad (14)$$

For the general box section shown in Fig. 8, its free torsion constant $I_{t,box}$ can be obtained from Eq. (15), and its sectorial moment of inertia $I_{\omega,box}$ can be obtained from Eq. (16). According to Eq. (16), when $b_1 = b_2$ and $t_1 = t_2$, then $I_{\omega,box} = 0$, that is, the sectorial moment of inertia of square steel pipe $I_{\omega,s} = 0$.

$$I_{t,box} = 2b_1^2 b_2^2 / (b_1 / t_1 + b_2 / t_2) \quad (15)$$

$$I_{\omega,box} = \frac{b_1^2 h^2 (t_1 b_1 + t_2 b_2) (t_2 b_1 - t_1 b_2)^2}{24(t_2 b_1 + t_1 b_2)^2} \quad (16)$$

By substituting the design parameters of CCSC into Eq. (11), the free torsion constant of CCSC section I_t can be obtained, as shown in Eq. (17).

$$I_t = (b_{st} - t_{st})^3 t_{st} + \left(4b_f t_f^3 + 4b_{cw} t_{cw}^3 \right) / 3 \quad (17)$$

The section of CCSC is approximately a cross biaxial symmetric section, and a group of flange and corrugated plate sections can be intercepted as a calculation unit, as shown in Fig. 9a. The specific simplified form of section and the main sectorial coordinates are shown in Fig. 9b. Point S is the shear center. The section of square steel pipe is only used as a reference for the section position of flange and corrugated plate in the schematic diagram, and it does not participate in the correlation calculation of sectorial moment of inertia in the calculation unit. Based on the general Eq. (14), Eq. (18) can be obtained to determine the sectorial moment of inertia of the flange section $I_{\omega,f}$. The values of d_{co} vary with the height of the column, but no matter whether it is positive, negative or 0, it does not affect the expression of sectorial moment of inertia. To simplify the calculation, the equivalent average value \bar{d}_{co} within a single waveform period is taken to participate in the calculation, as shown in Eq. (19).

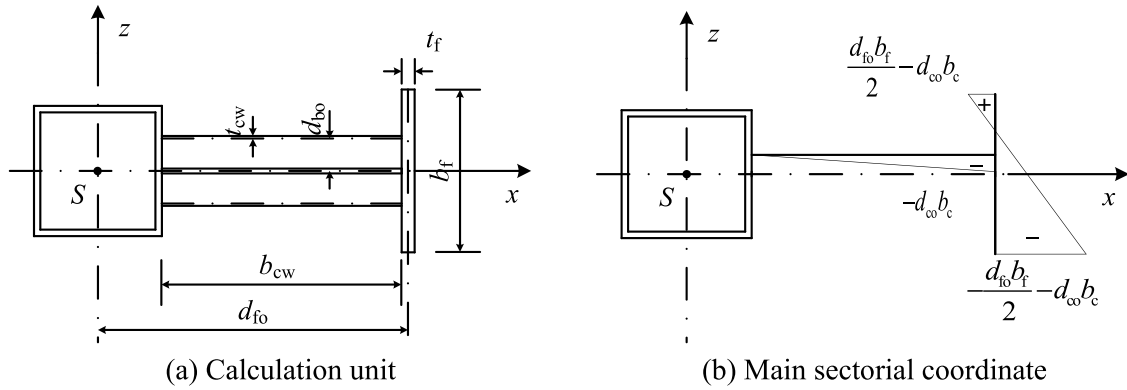
Fig. 9. I_{ω} and the main sectorial coordinates of a single unit of the CCSC.

Table 3
The auxiliary model parameters of $k_{cr,nt}$.

Model	H_c (mm)	b_{st} (mm)	t_{st} (mm)	b_f (mm)	t_f (mm)	b_{cw} (mm)	t_{cw} (mm)	f_y (MPa)	α_{st}	α_f	$\lambda_{\omega,n}$
TB1_1~6	3000~6000	100	5	200	16	200	2.5	345	18	7.4	6~13
TB2_1~6	3000~6000	100	5	150	12	200	2.5	345	18	7.8	6~13
TB3_1~6	6000~9000	80	4	100	8	240	2.5	345	18	8.6	12~19
TB4_1~6	6000~9000	80	4	200	16	240	2.5	345	18	7.4	11~17
TB5_1~6	6000~9000	80	4	100	8	360	3.0	345	18	8.6	9~14
TB6_1~6	6000~9000	80	4	80	8	420	3.0	345	18	7.3	8~12
TB7_1~6	6000~9000	80	4	80	8	540	3.0	345	18	7.3	6~10
TB8_1~6	6000~9000	80	4	100	8	360	3.0	235	18	8.6	9~14
TB9_1~6	6000~9000	80	4	80	8	540	3.0	390	18	7.3	6~10
TB10_1~6	6000~9000	80	3	100	8	240	2.0	345	25	8.6	11~18
TB11_1~6	6000~9000	120	4	200	12	240	2.0	345	28	9.9	10~16

$$\begin{aligned}
 I_{of} &= \frac{1}{3} \left[\left(\frac{d_{fo}(b_f - 2d_{co})}{2} - d_{co}b_{cw} \right)^2 + \left(\frac{d_{fo}(b_f - 2d_{co})}{2} - d_{co}b_{cw} \right) \cdot \left(-\frac{d_{fo}(b_f + 2d_{co})}{2} - d_{co}b_{cw} \right) \right. \\
 &\quad \left. + \left(-\frac{d_{fo}(b_f + 2d_{co})}{2} - d_{co}b_{cw} \right)^2 \right] t_f b_f \\
 &= \frac{t_f d_{fo}^2 b_f^3}{12} + d_{fo}^2 d_{co}^2 t_f b_f + d_{co}^2 b_{cw}^2 t_f b_f + 2d_{fo} d_{co}^2 b_{cw} t_f b_f
 \end{aligned} \tag{18}$$

$$\overline{d_{co}} = \sqrt{\int_0^{q_{cw}} d_{co}^2 dy / q_{cw}} = \sqrt{\left[a_{cw}^2 \int_0^{q_{cw}} \sin^2\left(\frac{2\pi}{q_{cw}} y\right) dy \right] / q_{cw}} = \frac{a_{cw}}{\sqrt{2}} \tag{19}$$

The sectorial moment of inertia of CCSC I_{ω} is the sum of I_{os} and I_{of} , as shown in Eq. (20). The sectorial moment of inertia of steel pipe I_{os} can be ignored.

$$\begin{aligned}
 I_{\omega} &= 4I_{of} + I_{os} = 4I_{of} \\
 &= \frac{t_f d_{fo}^2 b_f^3}{3} + 4d_{fo}^2 \overline{d_{co}}^2 t_f b_f + 4\overline{d_{co}}^2 b_{cw}^2 t_f b_f + 8d_{fo} \overline{d_{co}}^2 b_{cw} t_f b_f
 \end{aligned} \tag{20}$$

4.3.2. Theoretical calculation equation of torsional buckling critical load

The axial compression torsion buckling deformation is mainly composed of free torsion deformation and warping deformation. For the column with a conventional section, the torsional instability critical load $N_{cr0,nt}$ is calculated by Eq. (21). Considering the influence of corrugated plates and boundary conditions on the calculation, the adjustment factor of torsional buckling critical load $k_{cr,nt}$ is used to calculate the elastic torsional buckling critical load $N_{cr,nt}$ of CCSC, as shown in Eq. (22), where i_0 represents the torsional turning radius to the shear center, and

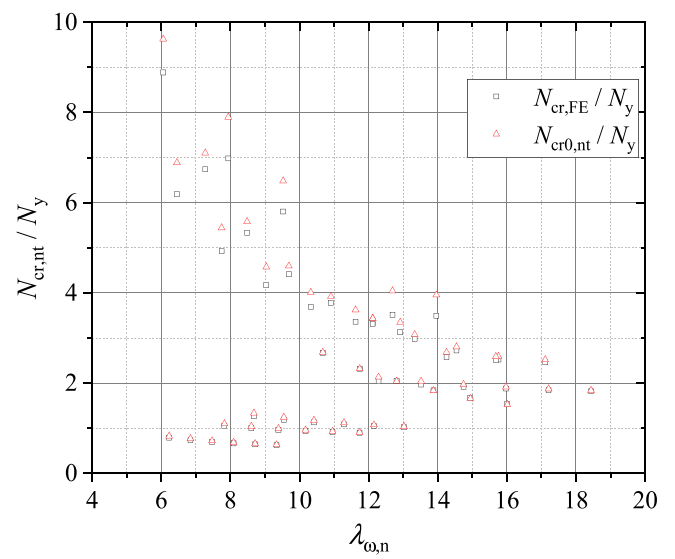


Fig. 10. Elastic stability factor.

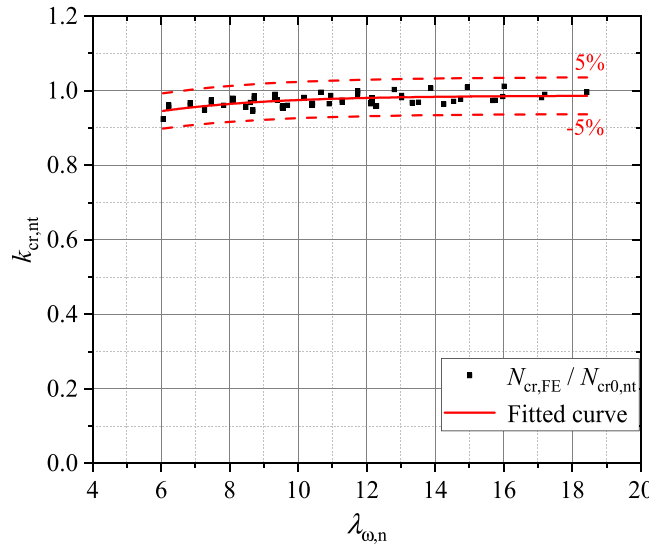
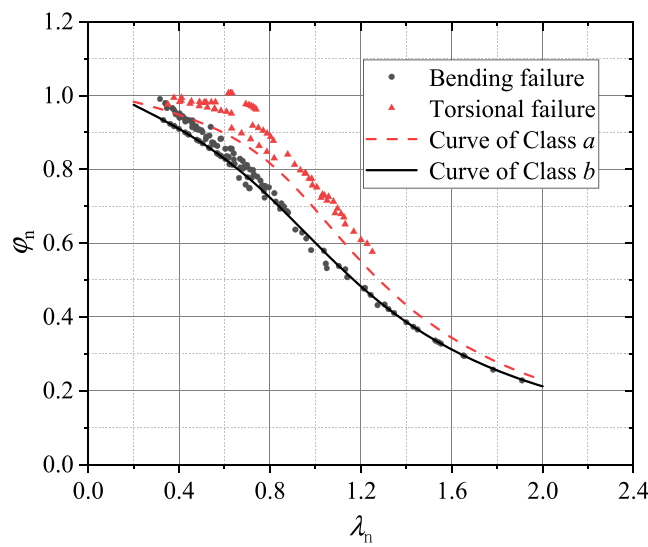
Fig. 11. Fitting process of $k_{cr,nt}$.

Fig. 12. Overall stability factor of CCSC.

$l_{0\omega}$ is the effective length of the column while considering the warping deformation boundary conditions. The calculation method of l_0 is shown in Eq. (23). The corrugated plate is ignored in the calculation process, that is, the values of three parameters I_x , I_z and A_{net} are not distinguished from that in Section 4.2.1.

$$N_{cr,nt} = \left(GI_t + \frac{\pi^2 EI_\omega}{l_{0\omega}^2} \right) / t_0^2 \quad (21)$$

$$N_{cr,nt} = k_{cr,nt} \cdot N_{cr,nt} \quad (22)$$

$$t_0^2 = (I_x + I_z) / A_{net} = 2I_x / A_{net} \quad (23)$$

4.3.3. Adjustment factor of torsional buckling critical load

The results of numerical simulation and theoretical calculation are compared and analyzed. The models designed according to Table 3 are used for data fitting of the adjustment factor of torsional buckling critical load $k_{cr,nt}$. Each group contains six models, and the torsional slenderness ratio $\lambda_{\omega,n}$ shown in Eq. (24) is taken as the main variable parameter. The specific variable parameters are b_{st} , t_{st} , b_f , t_f , b_{cw} , t_{cw}

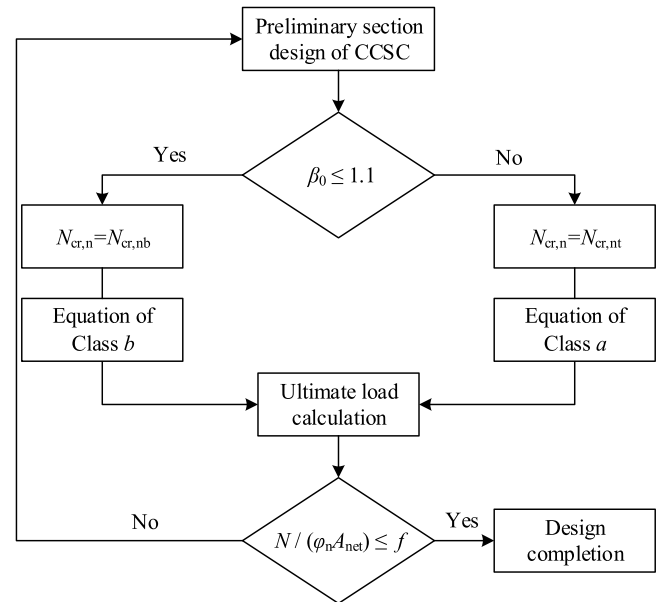


Fig. 13. Axial compression design process of CCSC.

 f_y .

$$\lambda_{\omega,n} = l_{0\omega} / i_0 \quad (24)$$

The comparison between $N_{cr,nt}$ and the finite element simulation result of torsional buckling critical load $N_{cr,FE}$ of CCSC is shown in Fig. 10. The ratio of numerical simulation results $N_{cr,FE}$ to the conventional equation results $N_{cr,nt}$ is represented by the factor $k_{cr,nt}$. The torsional slenderness ratio $\lambda_{\omega,n}$ is taken as the main variable to fitting the calculation equation of factor $k_{cr,nt}$, as shown in Eq. (25). The calculation error is kept within 5%, as shown in Fig. 11, which shows that the theoretical equation has good calculation precision.

$$k_{cr,nt} = 1.01 - 0.42 \times 0.88^{\lambda_{\omega,n}} \quad (25)$$

5. Design method of axial compression stability

5.1. Overall stability factor

Referring to the calculation method of the overall stability factor of axial compression column in GB50017-2017 "Standard for design of steel structures", the normalized slenderness ratio λ_n of the elongated column is calculated by using the slenderness ratio, and then the overall stability factor of axial compression of CCSC φ_n is obtained by calculating or looking up the table according to the code. The relationship between the ultimate axial load N_u and the stability factor φ_n of CCSC should satisfy Eq. (26). The calculation method of normalized slenderness ratio λ_n is shown in Eq. (27), where $N_{cr,n}$ is the critical load of elastic instability of axial compression column. If the first elastic buckling mode is flexural buckling, $N_{cr,n} = N_{cr,nb}$; if the first elastic buckling mode is torsional buckling, $N_{cr,n} = N_{cr,nt}$, as shown in Eq. (28). According to the first buckling mode obtained in the buckling analysis of the models mentioned in Sections 4.2 and 4.3, an initial geometric imperfection with $H_c/500$ is applied to the model. Axial static loading is carried out to obtain the ultimate load N_u of each model while considering the influence of the initial geometric imperfection.

Fig. 12 presents the correlation distribution between the overall stability factor φ_n of axial compression and the normalized slenderness ratio λ_n of CCSC. The stability factor curves of columns of Class a and Class b are drawn in the figure according to GB50017-2017 "Standard for design of steel structures" [16]. As can be seen from the figure, when the instability modes of axial compression columns are different, the

Table 4

Design parameters of the random check models.

Model	H_c (mm)	b_{st} (mm)	t_{st} (mm)	b_f (mm)	t_f (mm)	b_{cw} (mm)	t_{cw} (mm)	f_y (MPa)	β_0	Failure mode	λ_n	φ_n	$\varphi_{n,FE}$
RC-1	6000	120	6	150	12	200	2.5	345	0.803	Flexural	0.507	0.869	0.907
RC-2	6000	120	6	250	20	240	2.5	345	1.400	Torsional	0.494	0.931	0.966
RC-3	6000	120	6	200	16	120	2.0	345	0.404	Flexural	0.629	0.815	0.799
RC-4	4800	160	8	300	24	300	3.0	345	1.270	Torsional	0.367	0.959	0.963
RC-5	4800	160	8	200	16	200	2.5	345	0.771	Flexural	0.401	0.909	0.952
RC-6	4800	160	8	100	8	200	2.5	345	0.198	Flexural	0.493	0.875	0.936
RC-7	8400	100	5	150	12	200	2.5	345	0.794	Flexural	0.680	0.790	0.813
RC-8	8400	100	5	250	20	240	2.5	345	1.400	Torsional	0.650	0.884	0.913
RC-9	8400	100	5	200	16	120	2.0	345	0.344	Flexural	0.886	0.672	0.662
RC-10	9000	100	5	100	8	120	2.0	235	0.0778	Flexural	0.954	0.630	0.613
RC-11	9000	100	5	250	20	240	2.0	235	1.320	Torsional	0.552	0.912	0.945
RC-12	9000	100	5	200	16	80	2.0	235	0.145	Flexural	0.971	0.619	0.545
RC-13	9000	100	5	300	24	360	2.0	235	2.104	Torsional	0.527	0.919	0.920
RC-14	12,000	160	8	200	16	360	2.0	390	0.948	Flexural	0.629	0.815	0.973
RC-15	12,000	160	8	100	8	100	2.0	390	0.009	Flexural	1.733	0.273	0.275
RC-16	12,000	160	8	300	24	100	2.0	390	0.118	Flexural	1.191	0.488	0.460
RC-17	12,000	160	8	100	8	200	2.0	390	0.035	Flexural	1.224	0.470	0.466
RC-18	15,000	100	5	200	16	120	2.0	390	0.135	Flexural	1.672	0.289	0.283

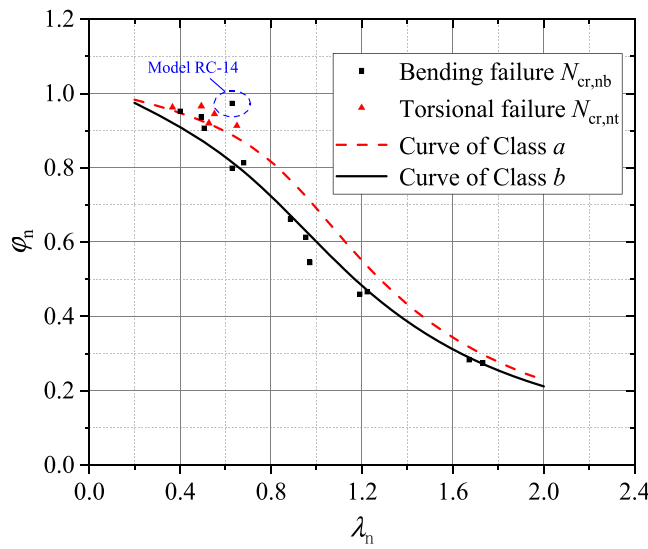


Fig. 14. Stability factor of random check models.

stability factor φ_n and normalized slenderness ratio λ_n show a different correlation. For the models with torsional instability, the correlation between φ_n and λ_n is also different, and this is because that different elastic buckling load ratio ($N_{cr,nb}/N_{cr,nt}$) of cross-section members will have influence on the change trend of torsional behavior [43].

When the axial compression flexural instability of the column occurs, the stability factor is in good agreement with the Class *b* column curve given in the code. The stability factor can be calculated by Eq. (29) [16]. When the axial compression torsional instability of the column occurs, the stability factor of all models is slightly higher than the stability factor of Class *a* column curve in the code. For convenient design, the stability factor for torsional instability members biased toward safety can be calculated by Eq. (30) [16].

$$\varphi_n = N_u/N \quad (26)$$

$$\lambda_n = \sqrt{\frac{N_y}{N_{cr,n}}} \quad (27)$$

$$N_{cr,n} = \min(N_{cr,nb}, N_{cr,nt}) \quad (28)$$

$$\varphi_n = \frac{1}{2\lambda_n^2} \left[(0.965 + 0.300\lambda_n + \lambda_n^2) - \sqrt{(0.965 + 0.300\lambda_n + \lambda_n^2)^2 - 4\lambda_n^2} \right] \quad (\text{Class b}) \quad (29)$$

$$\varphi_n = \frac{1}{2\lambda_n^2} \left[(0.986 + 0.152\lambda_n + \lambda_n^2) - \sqrt{(0.986 + 0.152\lambda_n + \lambda_n^2)^2 - 4\lambda_n^2} \right] \quad (\text{Class a}) \quad (30)$$

5.2. Design process

Fig. 13 shows the design process of the axial compression stability of CCSC. The section of CCSC is formulated preliminarily according to the design requirements. The instability mode of the CCSC is judged according to the design parameter values. Then, the ultimate axial compressive load of CCSC is calculated. The bearing capacity is verified by Eq. (31), where N represents the design value of axial compression load of the column. If the requirements are met, the design is completed; if not, the design parameters should be reconsidered.

The failure mode of CCSC can be judged by the instability mode influence coefficient $\beta_0 = N_{cr,nb}/N_{cr,nt}$. When the net section area of the CCSC under compression is similar, the bearing capacity of the torsional unstable column is significantly higher than that of the flexural unstable column. In addition, the processing and calculation errors exist in the actual situation. Thus, considering the structural safety, it is suggested that when $\beta_0 \leq 1.1$, the axial compression column is considered to have flexural instability, and when $\beta_0 \leq 1.1$ the axial compression column is considered to have torsional instability, so as to ensure the safety of the structure.

$$\frac{N}{N_u} = \frac{N}{\varphi_n N_y} = \frac{N}{\varphi_n f_y A_{net}} < 1.0 \quad (31)$$

Based on the above, the design equation of axial compression for CCSC can be obtained, as shown in Eq. (32), where f is the design value of steel strength after considering the material component factors.

$$\frac{N}{\varphi_n A_{net}} \leq f \quad (32)$$

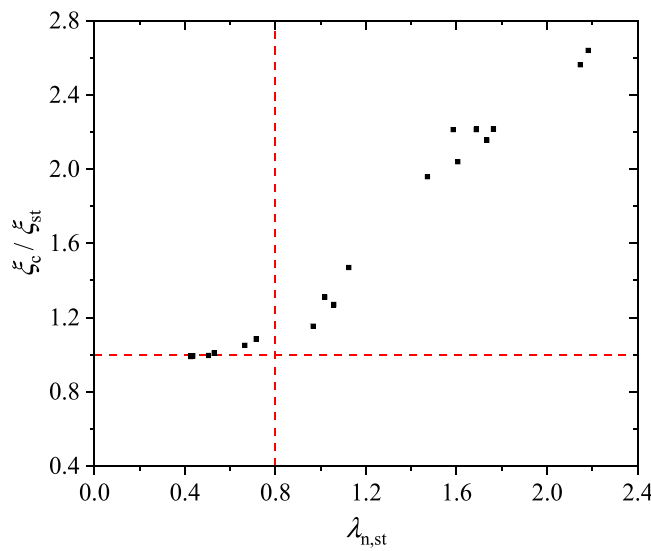
5.3. Design theory verification

A group of random checking models are designed, and the theoretical equation results of ultimate axial load are compared with the finite element simulation results. The relevant design parameters and calcu-

Table 5

Parameters and comparative results of contrastive analysis models.

Model	H_c (mm)	b_{st} (mm)	t_{st} (mm)	b_f (mm)	t_f (mm)	b_{cw} (mm)	t_{cw} (mm)	f_y (MPa)	λ_n	$\lambda_{n,st}$	A_{ret} (dm ²)	V_{total} (dm ³)	φ_n	ξ (kN/dm ³)	ξ_c/ξ_{st}
CE_1-C	3000	100	5	200	16	100	1.5	235	0.34	—	1.47	46.18	0.933	69.79	—
CE_1-A	3000	200	20	—	—	—	—	235	—	0.44	1.44	43.20	0.896	70.21	0.994
CE_1-V	3000	205	21	—	—	—	—	235	—	0.43	1.55	46.37	0.900	70.49	0.990
CE_2-C	3000	100	5	200	16	150	1.5	345	0.27	—	1.47	47.22	0.928	99.65	—
CE_2-A	3000	200	20	—	—	—	—	345	—	0.53	1.44	43.2	0.860	98.90	1.008
CE_2-V	3000	210	21	—	—	—	—	345	—	0.50	1.59	47.63	0.870	100.09	0.996
CE_3-C	3000	100	5	150	12	100	1.5	345	0.38	—	0.91	29.38	0.901	96.24	—
CE_3-A	3000	150	17	—	—	—	—	345	—	0.71	0.90	27.13	0.772	88.75	1.084
CE_3-V	3000	160	17	—	—	—	—	345	—	0.67	0.97	29.17	0.797	91.70	1.050
CE_4-C	6000	100	5	200	16	240	2.0	390	0.41	—	1.47	101.53	0.890	50.25	—
CE_4-A	6000	200	20	—	—	—	—	390	—	1.12	1.44	86.40	0.526	34.17	1.470
CE_4-V	6000	220	21	—	—	—	—	390	—	1.02	1.67	100.30	0.590	38.35	1.310
CE_5-C	6000	100	5	200	16	360	2.0	345	0.28	—	1.47	108.19	0.881	41.29	—
CE_5-A	6000	200	20	—	—	—	—	345	—	1.06	1.44	86.4	0.565	32.52	1.270
CE_5-V	6000	220	23	—	—	—	—	345	—	0.97	1.81	108.74	0.622	35.78	1.154
CE_6-C	6000	80	4	100	8	100	1.5	345	0.87	—	0.442	30.66	0.679	33.72	—
CE_6-A	6000	120	10	—	—	—	—	345	—	1.73	0.44	26.4	0.272	15.65	2.155
CE_6-V	6000	120	12	—	—	—	—	345	—	1.76	0.52	31.10	0.265	15.22	2.216
CE_7-C	9000	100	5	200	16	200	2.0	345	0.67	—	1.47	148.96	0.788	26.83	—
CE_7-A	9000	200	20	—	—	—	—	345	—	1.59	1.44	129.60	0.316	12.12	2.213
CE_7-V	9000	215	21	—	—	—	—	345	—	1.47	1.63	146.66	0.357	13.69	1.960
CE_8-C	9000	100	5	200	16	150	1.5	390	0.87	—	1.47	141.67	0.677	27.38	—
CE_8-A	9000	200	20	—	—	—	—	390	—	1.69	1.44	129.60	0.285	12.37	2.214
CE_8-V	9000	210	21	—	—	—	—	390	—	1.61	1.59	142.88	0.310	13.42	2.040
CE_9-C	9000	80	4	100	8	100	1.5	235	1.27	—	0.44	45.99	0.554	12.49	—
CE_9-A	9000	120	10	—	—	—	—	235	—	2.15	0.44	39.60	0.187	4.87	2.563
CE_9-V	9000	120	12	—	—	—	—	235	—	2.18	0.52	46.66	0.181	4.73	2.640

**Fig. 15.** Axial compression performance comparison.

lation results are shown in [Table 4](#) and [Fig. 14](#), where φ_n represents the stability factor calculated by [Eq. \(29\)](#) or [Eq. \(30\)](#), and $\varphi_{n,FE}$ represents the stability factor obtained by numerical simulation. Combined with the chart, it can be seen that the torsional instability of model RC-14 occurs in the finite element simulation, which is inconsistent with the theoretical equation result. The load value obtained by theoretical equation is obviously smaller than the simulation result, which conforms to the safety formulation principle of the design method in [Section 5.2](#). In summary, the theoretical equation results of axial compression stability factor of CCSC are basically consistent with the finite element simulation results, or are on the safe side, and the errors are in a reasonable range. Combined with the safety factor requirements set by steel structure design standards, the design method of axial compression stability of CCSC proposed in this paper can fully meet the requirements of the code for structural safety.

5.4. Applicability analysis

The CCSC sacrifices a small amount of bearing materials to bring great improvement to the overall stability. When the bearing capacity income brought by the stability improvement is larger than the bearing capacity loss caused by the reduction in the bearing section, the selection of CCSC can bring more economic benefits within the design requirements. In this paper, the square steel pipe column is used as the design basis for the stability strengthening analysis of axial compression.

Table 6
Design of the parameter analysis models.

Model	H_c (mm)	b_{st} (mm)	t_{st} (mm)	b_f (mm)	t_f (mm)	b_{cw} (mm)	t_{cw} (mm)	f_y (MPa)	α_{st}	α_f
PA1_1~6	6000	100	5	120~170	12	100	2.0	345	18	6.5~8.6
PA2_1~6	6000	100	5	200	15~20	100	2.0	345	18	7.9~5.9
PA3_1~6	6000	100	5	200	16	100~200	2.5	345	18	7.4
PA4_1~6	6000	80	4	200	12	120~220	2.5	345	18	9.9
PA5_1~6	6000	80~180	4~9	150	12	220	2.5	345	18	7.8
PA6_1~6	6000~9000	80	4	100	8	200	3.0	345	18	8.6
PA7_1~3	6000	100	5	200	16	100	1.0~3.0	345	18	7.4
PA8_1~3	6000	80	4	200	12	220	1.0~3.0	345	18	9.9

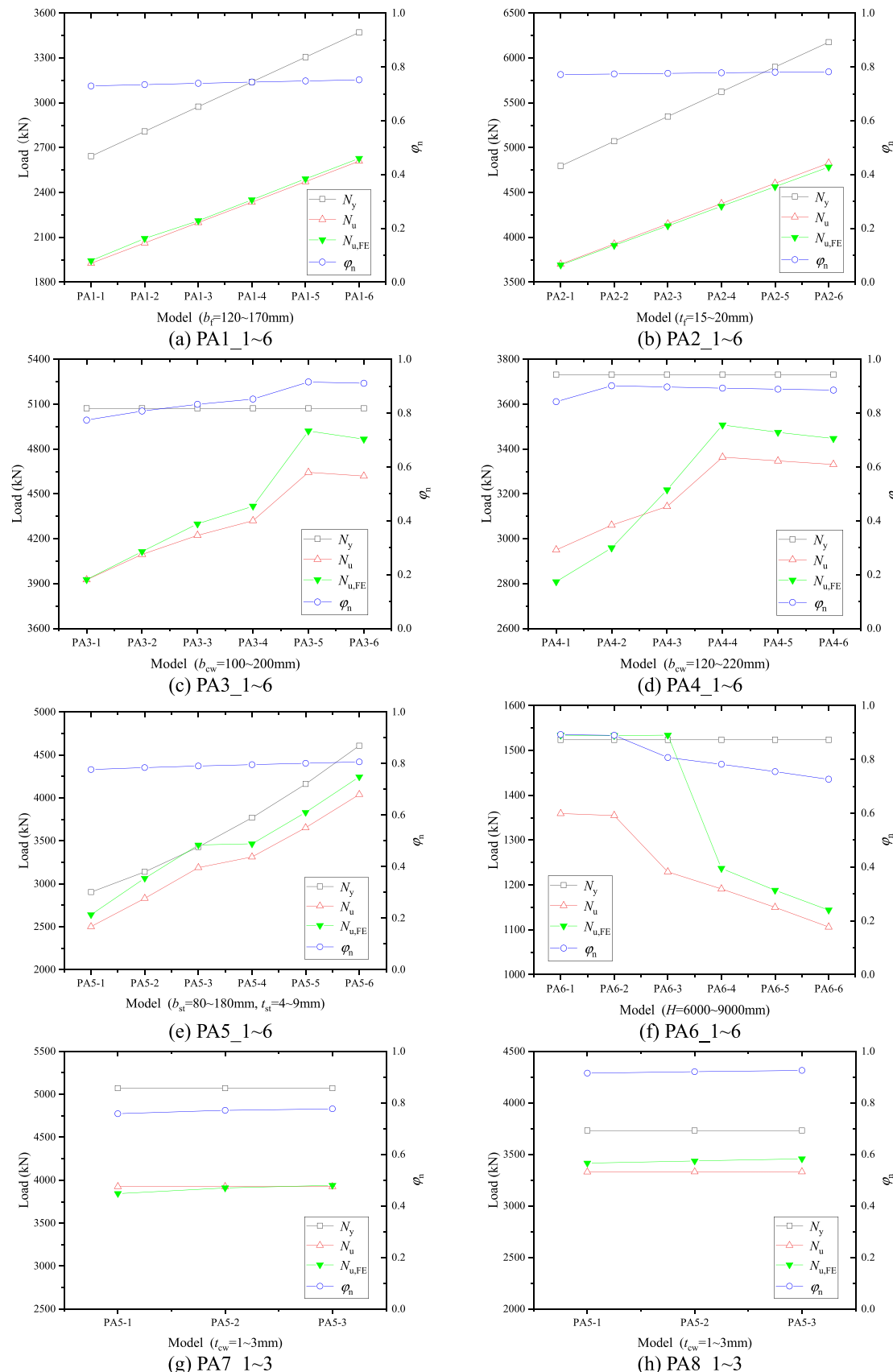


Fig. 16. Yield load, ultimate load and stability factor of the studied models.

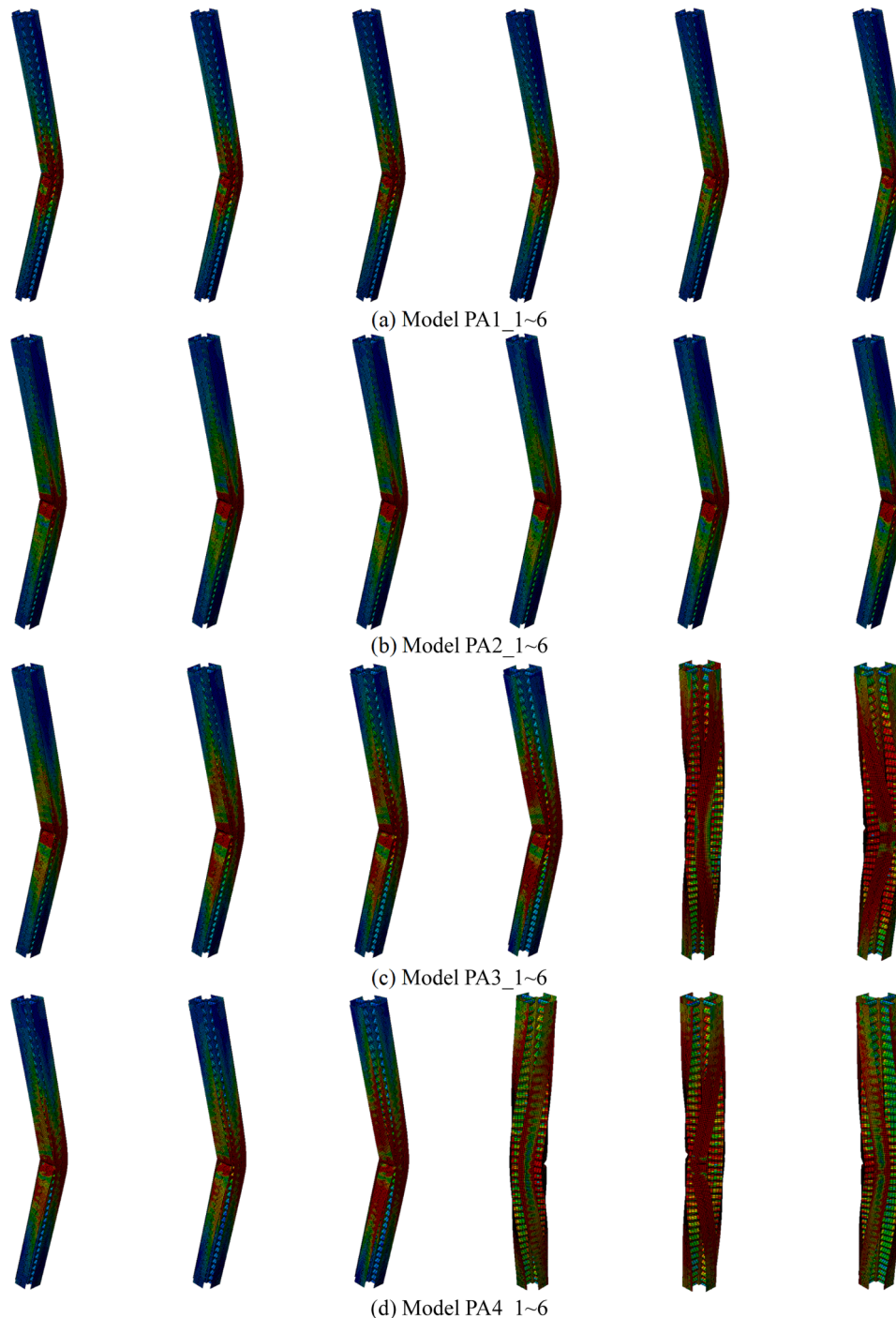


Fig. 17. Failure mode of the studied models.

One of the main features of special-shaped columns is the ability to avoid protruding from the wall. With this as the main design objective, 9 groups of control models of axial compression strength are designed. Each group of models includes 1 CCSC model and 2 square steel pipe models, and the section height of the steel pipe model is basically consistent with the width of the CCSC flange. Model CE-C represents the CCSC, model CE-A represents the square steel pipe with a net section area similar to that of the CCSC of the same group, and model CE-V is the square steel pipe with an overall steel volume similar to that of the CCSC of the same group. The design parameters and related calculation results of each model are shown in Table 5. Here, V_{total} represents the total

volume of each model, which should be calculated through the equivalent area of the full section A_{equ} , as shown in Eq. (33). The normalized slenderness ratio of the square steel pipe $\lambda_{n,st}$ can be obtained by Eq. (34) given in the code. The parameter ξ represents the axial compression capacity provided by the unit steel amount of a column, as shown in Eq. (35), and φ_n represents the ratio of the axial compression capacity provided by unit steel amount of the CCSC and the square steel pipe.

$$V_{\text{total}} = A_{\text{equ}} \cdot H_c \quad (33)$$

$$\lambda_{n,st} = \frac{\lambda}{\pi} \sqrt{f_y/E} \quad (34)$$

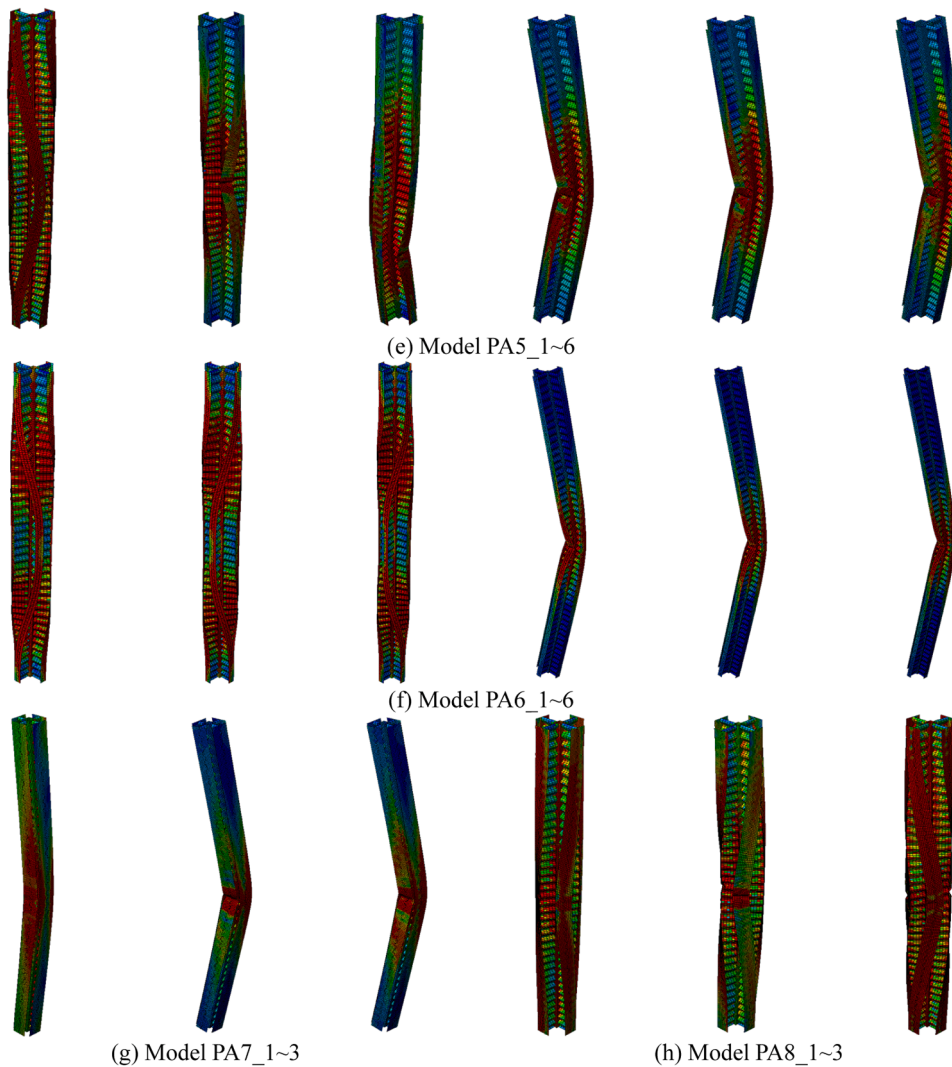


Fig. 17. (continued).

$$\xi = N_u / V_{\text{total}} \quad (35)$$

As can be seen from the table, in the groups of model CE_1~3, the difference of ultimate bearing capacity provided by the unit steel amount between CCSC and the square steel pipe is less than 10%. The ultimate bearing capacity provided by the unit steel amount of special-shaped column is obviously higher than that of square steel pipe in group CE_4~9. Fig. 15 shows the correlation distribution between ξ_c / ξ_{st} and $\lambda_{n,\text{st}}$. It can be seen that, with the goal of avoiding the structural column protruding from the wall, when the normalized slenderness ratio of square steel pipe $\lambda_{n,\text{st}}$ exceeds 0.8, significant economic improvement can be achieved by replacing it with a CCSC with a similar steel amount.

6. Parameter influence analysis

The six groups of models shown in Table 6 are designed to study the influence of flange plate width, flange plate thickness, corrugated plate width, and square steel pipe section size on the axial compression stability bearing capacity and instability mode of CCSC. Fig. 16 shows the variation trend of yield load N_y , ultimate load N_u , the numerical simulation results of ultimate load $N_{u,\text{FE}}$ and the axial compression stability factor φ_a of all models. In the figure, the hollow point represents the theoretical results, and the solid point represents the simulation results. Fig. 17 presents the failure modes of each model.

As can be seen from Fig. 16a~b and Fig. 17a~b, the flange width and

flange thickness can directly affect the net section area of CCSC under compression, and in turn influence the axial bearing capacity, but have little impact on the overall stability of the member, which can be basically ignored.

In Fig. 16c~d and Fig. 17c~d, flexural instability occurs on model PA3_1~4 and model PA4_1~3, and torsional instability occurs on model PA3_5 and model PA4_4~6. As can be seen from the figure, the width of the corrugated plate can significantly affect the section height of the column, and it plays a major role in controlling the overall axial pressure instability mode of the column. With the increase in the width of the corrugated plate, the bearing capacity of the flexural buckling column shows an upward trend, but the bearing capacity of the torsional buckling column shows a downward trend. When the instability mode changes from flexural to torsional, the bearing capacity will increase significantly and reach the peak value of the bearing capacity under the net bearing section parameter. The theoretical calculation results of model PA4_1 and PA4_2 are not on the safe side, but the calculation error is reasonably kept within 5%.

In Fig. 16e and Fig. 17e, torsional instability occurs on model PA5_1, torsional instability occurs on model PA5_2~3 at the initial yield stage while flexural instability occurs at the late loading stage, and flexural instability occurs on model PA5_4~6. On the whole, as the dimension of the core square steel pipe section increases, the overall instability mode of CCSC gradually changes from torsion to flexure. As a closed section, the

square steel pipe has a strong anti-warping ability and can obviously improve the anti-torsion ability of CCSC. As for model PA5_2~3, the two critical loads of elastic buckling of each model are similar, so torsional failure occurs at first and then flexural deformation occurs.

In Fig. 16f and Fig. 17f, torsional instability occurs on model PA6_1~3, while flexural instability occurs on model PA6_4~6. The numerical simulation results show that model PA6_1~3 with torsional instability has excellent stability, which is much higher than the theoretical calculation results. This is in line with the conclusion shown in Fig. 12 in that "the calculation results of Class a curve equation are safe for the CCSC with torsional instability". For model PA6_3, the numerical simulation results indicate that the model has torsional instability, while the theoretical calculation results reveal flexural instability with a smaller stability factor, indicating that when the CCSC is in the transition region between flexural and torsional instability, the instability mode judgment method proposed in this paper is conservative and safe. With the increase in column height, the instability mode of CCSC changes from torsional instability to flexural instability, and the stability factor of axial compression decreases continuously, which conforms to the variation rule of the stability factor of axial compression column. The overall stability of the column with flexural instability is more sensitive to the variation in column height.

In Fig. 16g~h and Fig. 17g~h, flexural instability occurs on model PA7_1~3, while torsional instability occurs on model PA8_1~3. As can be seen from Fig. 16g, the loading amplitude of model PA7_1 is smaller than that of other models, which is because the thickness of the corrugated plate is smaller than the requirement of the code, which cannot complete the whole loading process. It can be seen from the figure that the thickness of the corrugated plate has little influence on the bearing capacity of CCSC. So, the bearing capacity of corrugated plates can be ignored in the design and calculation process when the parameters can meet the requirements of the code.

7. Discussion

Based on the existing stability theory of steel structure, a new type of cross-section corrugated plate steel special-shaped column is proposed in this paper, and the corresponding calculation equations and design method of the overall stability factor are proposed. The proposed equations and curves are simplified for safety in this paper, and the design process is close to the content of the current standard, which further reduces the difficulty of using the design method by designers.

In this study, the section size of each plate meets the requirements of the section width-to-thickness ratio in the code GB50017–2017, so as to avoid the local failure of the plate. The overall height of CCSC is between 3m~12 m, the size of the square steel pipe is □80×4~□160×8, the size of the flange plate is 100×8~300×24, the waveform and thickness of the corrugated plate are obtained from the standard parameters given by the code T/CECS 290–2022[17], and the width of the corrugated plate is 80mm~550 mm, which can basically meet the needs of multi-high-rise building structure. Further research will be carried out in the future for the research on huge section columns or short columns less than 3 m, as well as corrugated plate special-shaped columns with other section shapes.

8. Conclusions

Based on the optimization design idea of the section of steel special-shaped column, a cross-section corrugated plate steel special-shaped column (CCSC) is proposed in this paper. The failure mode of the axial compression of CCSC is studied, the calculation equation of critical elastic buckling load of axial compression is derived, and the design method of axial compression stability is proposed. The main conclusions are as follows:

- 1 The proposed stability design method can effectively judge the buckling modes of the CCSC under axial compression. The overall stability factor of axial compression obtained from the design method is accurate and on the safe side.
- 2 The value of stability factor can be calculated according to the Class a column curve given by GB50017–2017 when torsional instability occurs in the CCSC. The value of stability factor can be calculated according to the Class b column curve given by GB50017–2017 when flexural instability occurs in the CCSC.
- 3 The rotating radius of CCSC can be adjusted freely by setting the width of corrugated plate. Increasing the width of corrugated plate can effectively improve the axial compression flexural stability but will reduce the axial compression torsional stability. For columns with good end torsion constraints, causing torsional instability of the column can effectively reduce the loss of bearing capacity.
- 4 The torsion resistance ability of the core square steel pipe can obviously affect the whole instability mode of CCSC, and increasing the free torsion constant of the square steel pipe can change the instability mode of CCSC from torsion to flexure.
- 5 The overall stability of CCSC decreases with the increase in column height. Short columns are prone to torsional instability, while long columns are prone to flexural instability, and the overall stability of the members with flexural instability is more significantly affected by column height.
- 6 With the design requirement of avoiding the structural column protruding from the wall, when the normalized slenderness ratio of square steel pipe exceeds 0.8, the CCSC has obvious advantages in terms of overall stability and steel consumption.

CRediT authorship contribution statement

Zi-qin Jiang: Writing – original draft, Project administration, Conceptualization. **Zi-yao Niu:** Writing – original draft, Investigation, Formal analysis. **Ai-Lin Zhang:** Project administration, Writing – original draft. **Xue-chun Liu:** Validation, Writing – review & editing.

Declaration of Competing Interest

Zi-qin Jiang, Zi-yao Niu, Ai-Lin Zhang and Xue-chun Liu declare that they have no conflict of interest.

Data availability

Data will be made available on request.

Acknowledgements

It is supported by the National Natural Science Foundation of China (Grant No. 52078013).

References

- [1] A.L. Zhang, The key issues of system innovation, drawing up standard and industrialization for modularized prefabricated high-rise steel structures, Ind. Constr. 44 (08) (2014) 1–6 ([in Chinese]).
- [2] Z.Y. Shen, Y.Q. Li, Discussion on promoting the development of steel building structure industry of China, Progress in Steel Building Structures 11 (04) (2009) 15–21 ([in Chinese]).
- [3] J.P. Hao, X.L. Sun, Q. Xue, C.L. Fan, Research and applications of prefabricated steel structure building systems, Eng. Mech. 34 (01) (2017) 1–13 ([in Chinese]).
- [4] F.C. Wang, L.H. Han, Analytical behavior of special-shaped CFST stub columns under axial compression, Thin-Walled Struct 129 (2018) 404–417.
- [5] W.B. Cui, L. Wang, H.R. Chen, H.T. Chen, S. Liu, The analysis on the seismic behavior of T-shaped prefabricated special-shaped CFST with rectangular multi-cell columns, Struct 28 (2020) 803–815.
- [6] X.G. Liu, C.Z. Xu, J.P. Liu, Y.L. Yang, Research on special-shaped concrete-filled steel tubular columns under axial compression, J. Constr. Steel Res. 147 (2018) 203–223.

- [7] C.F. Zhou, Y.J. Xue, Z.B. Hu, Z.Q. Liu, Coupled translational-torsional response for SRC frame with special-shaped columns under earthquake, *J. Build. Eng.* 31 (2020), 101440.
- [8] B.Y. Li, Y.L. Yang, J.P. Liu, X.G. Liu, Y. Chen, Y.F. Chen, Behavior of T-shaped CFST column to steel beam connection with U-shaped diaphragm, *J. Build. Eng.* 43 (2021), 102518.
- [9] Y.B. Wang, C. Bi, Z.L. Jiao, Z. Zhang, G.Q. Li, Experimental study on local stability of special-shaped HSS columns with single-corrugation, *J. Constr. Steel Res.* 201 (2023), 107726.
- [10] A.L. Zhang, J. Yu, M. Xu, J. Li, H.J. Liu, Experimental research on steel specially shaped columns with T-section under cyclic loading, *J. Build. Struct.* 31 (02) (2010) 20–28 ([in Chinese]).
- [11] A.L. Zhang, J. Yu, M. Xu, X.W. Liu, H.J. Liu, Experimental research on steel specially shaped columns with cruciform section under cyclic loading, *J. Build. Struct.* 31 (02) (2010) 11–19 ([in Chinese]).
- [12] M.L. Patton, K.D. Singh, Buckling of fixed-ended lean duplex stainless steel hollow columns of square, L-, T-, and +-shaped sections under pure axial compression - a finite element study, *Thin-Walled Struct.* 63 (2013) 106–116.
- [13] M.M. Nasrabadi, S. Torabian, S. R.Mirghaderi, Panel zone modelling of Flanged Cruciform Columns: an analytical and numerical approach, *Eng. Struct.* 49 (2013) 491–507.
- [14] M.A. Rendall, G.J. Hancock, K.J. R.Rasmussen, Modal buckling behaviour of long polygonal tubes in uniform torsion using the generalised cFSM, *Thin-Walled Struct.* 128 (2018) 141–151.
- [15] T. Zhou, Z.H. Chen, B.H. Liu, Seismic behavior of special shaped column composed of concrete filled steel tubes, *J. Constr. Steel Res.* 75 (2012) 131–141.
- [16] GB 50017-2017, Standard For Design of Steel Structures, China Architecture & Building Press, Beijing, 2017 ([in Chinese]).
- [17] T/CECS 290-2022, Technical Specification For Steel Corrugated-Plates Structures, China Planning Press, Beijing, 2022 ([in Chinese]).
- [18] Y.L. Guo, X.A. Wang, B.H. Zhang, Z.Q. Jiang, The state of the art design theory of sinusoidal web steel structures, *Ind. Constr.* 42 (07) (2012) 1–13 ([in Chinese]).
- [19] B. Jáger, L. Dunai, B. Kövesdi, Girders with trapezoidally corrugated webs subjected by combination of bending, shear and path loading, *Thin-Walled Struct.* 96 (2015) 227–239.
- [20] B. Kövesdi, L. Dunai, Fatigue life of girders with trapezoidally corrugated webs: an experimental study, *Int. J. Fatigue* 64 (2014) 22–32.
- [21] S.A. Ibrahim, Lateral torsional buckling strength of unsymmetrical plate girders with corrugated webs, *Eng. Struct.* 81 (2014) 123–134.
- [22] A. Shahmohammadi, R. Mirghaderi, M. Hajasadeghi, M. Khanmohammadi, Application of corrugated plates as the web of steel coupling beams, *J. Constr. Steel Res.* 85 (2013) 178–190.
- [23] R. Aydin, E. Yuksel, N. Yardimci, M.H. Kisa, T. Gokce, In-plane behaviour of beam-to-column connections of corrugated web I-sections, *J. Constr. Steel Res.* 100 (2014) 183–196.
- [24] E. Sayed-Ahmed, Behaviour of steel and (or) composite girders with corrugated steel webs, *Canadian J. Civil Eng.* 28 (4) (2001) 656–672.
- [25] S. Kudryavtsev, Buckling behavior of steel column with triangularly corrugated web, *MATEC Web Conf.* 279 (2019) 2007.
- [26] S.G. Morkhade, S.M. Baswaraj, C.B. Nayak, Comparative study of effect of web openings on the strength capacities of steel beam with trapezoidally corrugated web, *Asian J. Civil Eng.* 20 (8) (2019) 1089–1099.
- [27] X.Q. Lin, H. Far, X.T. Zhang, Shear Capacity Analysis of Welded Steel I-Girders with Corrugated Webs based on First Yield, *Int. J. Steel Struct.* 21 (3) (2021) 1053–1062.
- [28] Z.Q. Jiang, X.F. Yang, C. Dou, S.H. Li, A.L. Zhang, Seismic performance of prefabricated corrugated web beam-column joint with replaceable cover plates, *Adv. Struct. Eng.* 22 (5) (2019) 1161–1174.
- [29] Z.Q. Jiang, Z.Y. Niu, A.L. Zhang, X.C. Liu, S.H. Li, Experimental study of earthquake-resilient prefabricated sinusoidal corrugated web beam-column joint, *Thin-Walled Struct.* 144 (2019), 106306.
- [30] A.L. Zhang, S.H. Li, Z.Q. Jiang, H. Fang, C. Dou, Design theory of earthquake-resilient prefabricated sinusoidal corrugated web beam-column joint, *Eng. Struct.* 150 (2017) 665–673.
- [31] Y.L. Feng, L.Z. Jiang, W.B. Zhou, J.P. Han, Lateral-torsional buckling of box beam with corrugated steel webs, *J. Cent. South Univ.* 26 (7) (2019) 1946–1957.
- [32] M. Nassirnia, A. Heidarpour, X.L. Zhao, J. Minkkinen, Innovative hollow columns comprising corrugated plates and ultra high-strength steel tubes, *Thin-Walled Struct.* 101 (2016) 14–25.
- [33] S.N. Sadeghi, A. Heidarpour, X. Zhao, et al., An innovative I-beam to hybrid fabricated column connection: experimental investigation[J], *Engineering Structures.* 148 (2017) 907–923.
- [34] M. Nassirnia, A. Heidarpour, X.L. Zhao, A benchmark analytical approach for evaluating ultimate compressive strength of hollow corrugated stub columns, *Thin-Walled Struct.* 117 (2017) 127–139.
- [35] J.W. Berman, M. Bruneau, Experimental Investigation of Light-Gauge Steel Plate Shear Walls, *J. Struct. Eng.* 131 (2) (2005) 259–267.
- [36] F. Emami, M. Mofid, A. Vafai, Experimental study on cyclic behavior of trapezoidally corrugated steel shear walls, *Eng. Struct.* 48 (2013) 750–762.
- [37] F. Emami, M. Mofid, On the hysteretic behavior of trapezoidally corrugated steel shear walls, *Struct. Des. Tall Spec.* 23 (2) (2014) 94–104.
- [38] Q. Cao, J.Y. Huang, Experimental study and numerical simulation of corrugated steel plate shear walls subjected to cyclic loads, *Thin-Walled Struct.* 127 (2018) 306–317.
- [39] Y. Yadollahi, I. Pakar, M. Bayat, Evaluation and comparison of behavior of corrugated steel plate shear walls, *Lat. Am. J. Solids Stru.* 12 (4) (2015) 763–786.
- [40] ABAQUS, Standard User's Manual Version 6.10, Hibbit, Karlsson & Sorensen, Inc, Pawtucket, RI, 2010.
- [41] H. Achref, M. Foudil, D. Noureddine, Analytical and finite element analyses of flexural and torsional buckling of I-columns with discrete braces, *Thin-Walled Struct.* 174 (2022), 109100.
- [42] Y.Q. Wang, H.X. Yuan, T. Chang, X.X. Du, M. Yu, Compressive buckling strength of extruded aluminium alloy I-section columns with fixed-pinned end conditions, *Thin-Walled Struct.* 119 (2017) 396–403.
- [43] B. Behzadi-Sofiani, L. Gardner, M.A. Wadee, Behaviour, finite element modelling and design of cruciform section steel columns, *Thin-Walled Struct.* 182 (2023), 110124.